NMR Backbone Dynamics of VEK-30 Bound to the Human Plasminogen Kringle 2 Domain

Min Wang, Mary Prorok, and Francis J. Castellino*
W. M. Keck Center for Transgene and the Department of Chemistry and Biochemistry, University of Notre Dame, Notre Dame, Indiana

ABSTRACT To gain insights into the mechanisms for the tight and highly specific interaction of the kringle 2 domain of human plasminogen ($K2_{Pg}$) with a 30-residue internal peptide (VEK-30) from a group A streptococcal M-like protein, the dynamic properties of free and bound $K2_{Pg}$ and VEK-30 were investigated using backbone amide ^{15}N-NMR relaxation measurements. Dynamic parameters, namely the generalized order parameter, S^2, the local correlation time, τ_e, and the conformational exchange contribution, R_{ex}, were obtained for this complex by Lipari-Szabo model-free analysis. The results show that VEK-30 displays distinctly different dynamic behavior as a consequence of binding to $K2_{Pg}$, manifest by decreased backbone flexibility, particularly at the binding region of the peptide. In contrast, the backbone dynamics parameters of $K2_{Pg}$ displayed similar patterns in the free and bound forms, but, nonetheless, showed interesting differences. Based on our previous structure-function studies of this interaction, we also made comparisons of the VEK-30/$K2_{Pg}$ dynamics results from different kringle modules complexed with small lysine analogs. The differences in dynamics observed for kringles with different ligands provide what we believe to be new insights into the interactions responsible for protein-ligand recognition and a better understanding of the differences in binding affinity and binding specificity of kringle domains with various ligands.

INTRODUCTION

The group A streptococcal surface virulence protein, PAM, a 43 kDa member of the M-like protein family, interacts with high affinity and specificity with the lysine binding site (LBS) of the 80-residue kringle-2 (K2) domain of human plasminogen (hPg) (1). A region of PAM, spanning amino acid residues 91–116, contains its $\alpha1\alpha2$ repeat sequences, and is responsible for binding of PAM to the $K2_{Pg}$ domain, an event that allows for a proteolytic bacterial surface and heavily contributes to virulence of PAM+ group A streptococci (2). A functional internal peptide of PAM, namely VEK-30, derived from residues 85–113 of PAM, and containing the first and most of the second direct repeat, possesses a high-affinity binding site for $K2_{Pg}$ ($K_D = 460$ nM). In contrast, there is no measurable affinity of VEK-30 to any of the other isolated hPg kringles (3–5).

Recently, we determined the NMR structures of the VEK-30/$K2_{Pg}$ complex, which provided an understanding the intermolecular interactions that govern this interaction in solution (6). On the basis of the solution structure, as well as multiple sequence alignments of different kringle modules, and mutational studies, we proposed that the conserved hydrophobic binding core of $K2_{Pg}$ (residues Tyr^{35}, Phe^{40}, Trp^{60}, Phe^{62}, Trp^{70}, and Y^{72}), along with side chain residues in its anionic (Asp^{54} and Asp^{56}), and cationic (Arg^{69}) centers, interacts with VEK-30 in a similar fashion as its binding to small lysine analogs, resulting in a basal level of binding affinity. However, several nonconserved residues, including Gly^{34}, Lys^{39}, Lys^{43}, and Arg^{55}, which specifically exist in $K2_{Pg}$, and are located outside of the canonical LBS, strategically occupy specific positions that optimize interactions with VEK-30. These exosite interactions enhance affinity of VEK-30 to $K2_{Pg}$ and facilitate the docking of VEK-30 to the $K2_{Pg}$ domain by modulating ligand recognition and binding specificity.

Structural data alone are not sufficient for an in-depth prediction of binding properties (7–9). Internal dynamics commonly plays an important role in the function of proteins. For example, specific molecular recognition processes that occur in biological systems are dependent on the dynamic properties of the species involved. NMR spectroscopy is not only of great use for determining the atomic structures of proteins, but also is a powerful and unique tool for the study of dynamic properties of proteins at the atomic level (10–13). The dynamical analyses of relaxation data using the model-free approach introduce a global rotational correlation time (τ_m), an internal correlation time (τ_e), and an order parameter (S^2), the latter being related to the amplitudes of internal motions for each residue (14–16). These approaches are useful in furthering our understanding of the role of time-dependent conformational fluctuations involved in binding events, and provide insights into describing the contributions of motions on different timescales to the high affinity and binding specificity.

In this study, NMR relaxation data for both free and bound forms of VEK-30 and $K2_{Pg}$ were collected and analyzed with Lipari-Szabo model-free approaches to investigate the changes in backbone dynamics induced by binding of each peptide. These dynamics studies provide important complementary information regarding the nature of this specific molecular recognition event.

Submitted January 20, 2010, and accepted for publication April 8, 2010.

*Correspondence: fcastell@nd.edu

Editor: Patrick Loria.

0006-3495/10/07/0302/11 $2.00

doi: 10.1016/j.bpj.2010.04.019

METHODS

Protein expression and purification

^{15}N-$K2_{Pg}$[C4G/E56D/L72Y], a triple variant of wild-type (WT)-$K2_{Pg}$ that displays enhanced affinity for lysine analogs and VEK-30 compared to WT-$K2_{Pg}$ was expressed in *Pichia pastoris* GS115 cells and purified as described (6). Final yields of ^{15}N-$K2_{Pg}$ were typically 75–100 mg/L. ^{15}N-VEK-30 was expressed in *Escherichia coli* and purified as published (6). Final recoveries of peptide were 10–15 mg/L.

The purity and correct folding of materials were verified by SDS-PAGE and 2D HSQC spectroscopy, respectively. MALDI-TOF mass spectrometry was used for molecular weight analyses. For the uniformly labeled ^{15}N-peptides, single mass peaks were obtained at the correct molecular weights, indicating nearly complete incorporation of ^{15}N.

NMR sample preparations

Samples (1 mM) were dissolved in a buffer containing 50 mM Hepes (pH 7.0), 1 mM EDTA, 200 mM NaCl, 3 mM NaN_3, 10% ^2H_2O and 0.2 mM 2,2-dimethyl-2-silapentane-5-sulfonic acid. Samples of the binary complex were prepared at 1 mM (1:1 stoichiometry of VEK-30/$K2_{Pg}$).

NMR spectroscopy and backbone ^{15}N relaxation measurements

NMR spectra were collected on a Bruker AVANCE 800 MHz spectrometer using a 5-mm triple resonance cryoprobe. The backbone chemical-shift assignments were obtained by a set of 3D-HNCA, HNCO, HNCACB, HBHA(CO)NH, and CBCA(CO)NH experiments (6). Data were zero-filled to double the original data points and apodized with 90° to 60° shift square sine bell window function before Fourier transformation. ^1H and ^{15}N chemical shifts were referenced indirectly to internal 2,2-dimethyl-2-silapentane-5-sulfonic acid (17).

The backbone ^{15}N relaxation parameters, including longitudinal relaxation rates (R_1), transverse relaxation rates (R_2), and steady-state heteronuclear [^1H]-^{15}N NOEs, for free and complexed VEK-30 and $K2_{Pg}$ were measured using standard pulse sequences at 298 K. All ^{15}N-R_1 and ^{15}N-R_2 relaxation experiments were carried out in an interleave manner with a 2-s recycle delay between scans. The relaxation delays used for complexed and free $K2_{Pg}$ were 10×2, 100, 300, 500, 800, 1000, 1200, and 1600 ms for the R_1 experiments and were 17×2, 34, 51, 68, 85, 102, 119, 136, 153, 170, 204, and 238 ms for the R_2 experiments. For free VEK-30, relaxation delays were set to 10×2, 50, 90, 220, 350, 520, 680, 820, 960, and 1100 ms for the R_1 experiments and 17×2, 34, 51, 68, 85, 102, 119, 136, 153, 170, and 204 ms for the R_2 experiments. Duplicate spectra were used to estimate experimental errors. The relaxation rates were determined by fitting the crosspeak intensities to a single exponential function using nonlinear least-squares. The error in the rate constant was assessed from Monte Carlo simulations. [^1H]-^{15}N NOE experiments were carried out in the absence and presence of a 3-s proton saturation period before the ^{15}N excitation pulse, using recycle delays of 4 and 7 s. Heteronuclear NOE values were obtained from the ratios of the peak intensities measured with and without proton saturation. Peak intensities uncertainties were estimated from the noise level of the spectra (NOE measurements).

RESULTS

To investigate the motional properties of $K2_{Pg}$ and VEK-30, as well as to obtain further insights into the molecular mechanisms of their mutual recognition, backbone ^{15}N longitudinal relaxation rates (R_1), transverse relaxation rates (R_2), and heteronuclear ^1H-^{15}N NOE values, for free and bound peptides, were measured.

^{15}N relaxation measurements for $K2_{Pg}$

In these analyses, 66 and 69 of 87 residues were used for the free and the VEK-30 bound forms of $K2_{Pg}$, respectively. The unanalyzed residues included seven proline residues (Pro^{30}, Pro^{37}, Pro^{41}, Pro^{53}, Pro^{59}, Pro^{66}, and Pro^{76}) that have no amide protons. Other residues were excluded due to weak signals or severe spectral overlap. The experimental relaxation rates, R_1, R_2, and ^1H-^{15}N NOE values, are plotted against the amino acid sequence (Fig. S1 in the Supporting Material). Overall, the R_1, R_2, and NOE values of $K2_{Pg}$, complexed to VEK-30, show similar patterns in comparison to those of the apo form, i.e., there is little variation in R_1 value across the sequence of $K2_{Pg}$, and the R_2 rates exhibit clear differences between the bulk of protein and several regions. Further, a significant decrease in R_2 is observed at both the N- and C-termini. Relatively high NOE values appeared in the core region (1–78) with the large deviations from average values also observed at the two termini.

Average R_1, R_2, and NOE values of 1.34 s^{-1}, 11.9 s^{-1}, and 0.79, respectively, were obtained for free $K2_{Pg}$, and average R_1, R_2, and NOE values of 1.19 s^{-1}, 14.0 s^{-1}, and 0.80, respectively, were obtained for bound $K2_{Pg}$. The high backbone ^1H-^{15}N NOE values indicate that $K2_{Pg}$ is generally rigid on the ps timescale, both in its apo- and VEK-30-bound states. Residues in the two terminal segments of Tyr^7–Glu^1 and Asp^{74}–Ala^{80} showed relatively low R_2 and NOE values, indicating their high flexibility on the ps-ns timescale. These observations are consistent with the lack of observed medium- and long-range NOEs within these peptide regions, based on the NOE data (6). For both forms of $K2_{Pg}$, Gly^6, Cys^{22}, His^{31}, Ala^{32}, Lys^{39}, Thr^{63}, and Thr^{64} show larger than the average R_2/R_1 values, indicative of conformational exchanges on μs-ms timescale and/or internal motions on the ps-ns timescale. Notably, the segment Gly^{34}–Lys^{46} in the apo form manifests more fluctuations in R_2 rates than in the complexed state (Fig. S1).

^{15}N relaxation measurements for VEK-30

Reliable relaxation parameters were obtained for 26 and 25 of 32 nonproline residues for apo and bound VEK-30, respectively. The unanalyzed residues were due to partial overlap or line-broadening, indicative of internal motion and/or rapid exchange with solvent. The residue-specific relaxation parameters are shown in Fig. S2. Overall, the internal dynamics of VEK-30 complexed to $K2_{Pg}$ is significantly changed relative to apo-VEK-30. In the complex, the R_1 rates significantly decreased, and the R_2 rates systematically increased, compared with free VEK-30, in agreement with the almost three-fold increase in molecular mass of VEK-30 in the complex. The [^1H]-^{15}N NOE value of free VEK-30 is systematically low (average value $= 0.25 \pm 0.34$), compared to that of bound state (average value $= 0.60 \pm 0.33$), suggesting that the functional peptide is highly mobile and

unstructured in absence of $K2_{Pg}$, which is consistent with the chemical shift index of VEK-30. The complex structure determined by x-ray and NMR methods showed that VEK-30 adopts an extended α-helix conformation throughout residues Ala^{6}-Leu^{26}, whereas the N- and C-terminal regions are solvent exposed and structurally disordered. Most of the intermolecular interactions occur between a single face of the α-helix of VEK-30 (residues 6–21) and the LBS of $K2_{Pg}$. Consistent with the structure of VEK-30 in the complex, the bound peptide exhibits distinct differences in the relaxation parameters, R_2 and NOE in three regions. These include: N- and C-terminal residues, 1–5 and 27–30, respectively, which have lowest average R_2 ($5.5 \pm 2.1\ s^{-1}$); residues 6–21, which make the majority of close contacts with $K2_{Pg,}$ and have the highest average R_2 value ($13.6 \pm 1.4\ s^{-1}$); and residues 22–27, which is an extended α-helical region, and has slightly lower R_2 values than residues 6–21. Similarly, the different regions of the bound peptide clearly show different ranges of NOE values. Both the N- and C-terminal residues have negative, or relatively low, NOE values as compared to the average NOE for the remainder of the peptide. Unlike the other relaxation measurements, the different regions of the peptide did not exhibit systematic variations in R_1 values. Therefore, Fig. S2 indicates that binding of $K2_{Pg}$ perturbs the dynamics of VEK-30 by reducing backbone flexibility throughout the extended α-helix, more strikingly, at the main binding region of the residue 6–21 region, as demonstrated by changes in the overall patterns of the R_1, R_2, and NOE values plotted as a function of residue number.

Model-free analysis

The analysis of backbone dynamic parameters was carried out using the Lipari-Szabo model-free method, as implemented in the program, Tensor 2 (18). In this approach, relaxation rates were first used to estimate the diffusion tensor. Here, common procedures were followed to determine the rotational diffusion tensors of both apo-$K2_{Pg}$ and VEK-30/$K2_{Pg}$ by excluding residues with conformational exchanges and/or fast internal motions. Residues that satisfied these criteria were used to characterize the diffusion tensor, which was chosen over isotropic and anisotropic models. On the basis of the observation that the degree of anisotropy was found to be small ($D_{//}/D_{\perp} \approx 1.03$ and 1.06 for apo-$K2_{Pg}$ and VEK-30-bound $K2_{Pg}$, respectively) and the improvement in χ^2 was not meaningful according to a statistical F-test, the diffusion tensors were best defined by isotropic rotational tumbling for both apo-$K2_{Pg}$ and $K2_{Pg}$ bound to VEK-30, thus providing the initial estimate of global correlation times (τ_m) of 6.72 ± 0.02 ns and 7.80 ± 0.02 ns for free $K2_{Pg}$ and the $K2_{Pg}$/VEK-30 complex, respectively. The correlation times indicate that both forms of $K2_{Pg}$ are in the monomeric state under the NMR experimental conditions, which is in accord with analytical ultracentrifugation data that we reported earlier (6).

The model-free parameters were extracted using the experimentally determined ^{15}N relaxation rate parameters and the heteronuclear NOE values, and an isotropic diffusion model was used in the analysis. The amide bond length was fixed at 1.02 Å, and a ^{15}N chemical-shift anisotropy value of -175 ppm was used in the calculations. Five simplified models of internal mobility are defined. These are: model (M)1-S^2; model (M)2-S^2, τ_e; model (M)3-S^2, R_{ex}; model (M)4-S^2, τ_e, R_{ex}; model (M)5-S_f^2, S^2, τ_e. These models were iteratively used to fit the experimental data until the confidence reached 95% (19). Here, S^2 ($= S_f^2\ S_s^2$) is the square of the generalized order parameter characterizing the amplitude of the internal motions, where S_f^2 and S_s^2 are the squares of the order parameters for the internal motions on the fast and slow timescales, respectively. τ_e is the effective correlation time, which indicates the timescale of internal motions. The confidence levels were estimated using 300 Monte Carlo simulations per run in combination with χ^2 and F-test criteria. To take into account the contribution to the experimental ^{15}N R_2 relaxation rate from conformational exchange processes, an additional parameter (R_{ex}) was introduced. Using the model-free formalism, backbone amides were fitted to either one of the five models. Fig. S3 summarizes the number of residues that fit to each of the five models for both the apo- and VEK-30 bound $K2_{Pg}$. The optimized internal mobility parameters of the generalized order parameter, S^2, the fast internal motion on ps-ns timescales, τ_e, and the conformational exchange, R_{ex}, on μs-ms timescales are shown in Fig. 1 and Fig. 2.

Model-free analysis of backbone motions in $K2_{Pg}$

As shown in Fig. S3, after model selection, 34 residues for apo-$K2_{Pg}$ were described by M1 and 10 residues were fit to M2, indicating internal motions (τ_e) on ps-ns timescales. A total of 11 residues were fitted to M3 and six residues were assigned to M4, suggesting more complicated and flexible internal motions. Five residues were assigned to M5. There are three residues that could not be fit to any of these models. Of the bound $K2_{Pg}$ residues that were analyzed, 35 were fit to M1, 13 to M2, 11 to M3, 4 to M4, and 6 to M5. Two residues could not be fit to the five traditional models. Therefore, for both forms of $K2_{Pg}$, the majority of residues were best-fit with the simplest model, either with S^2 (M1) or S^2 and τ_e (M2). The extracted dynamic parameters (S^2, τ_e, and R_{ex}) for free and bound forms of $K2_{Pg}$, are reported in Fig. 1. Average S^2 values of 0.88 ± 0.10 and 0.91 ± 0.09 were obtained for the free and VEK-30-bound states of $K2_{Pg}$, respectively, indicating that the $K2_{Pg}$ domain, both in the absence and presence of VEK-30, shows similar restricted motions on ps-ns timescales (Fig. 3, *A* and *B*). For the core-region (residue 1–78), as compared in both states, $\Delta S^2_{bound\text{-}free}$ averages 0.028. This suggests that VEK-30 binding results in a slight enhancement of overall rigidity on the ps-ns timescale. Despite this fact, several

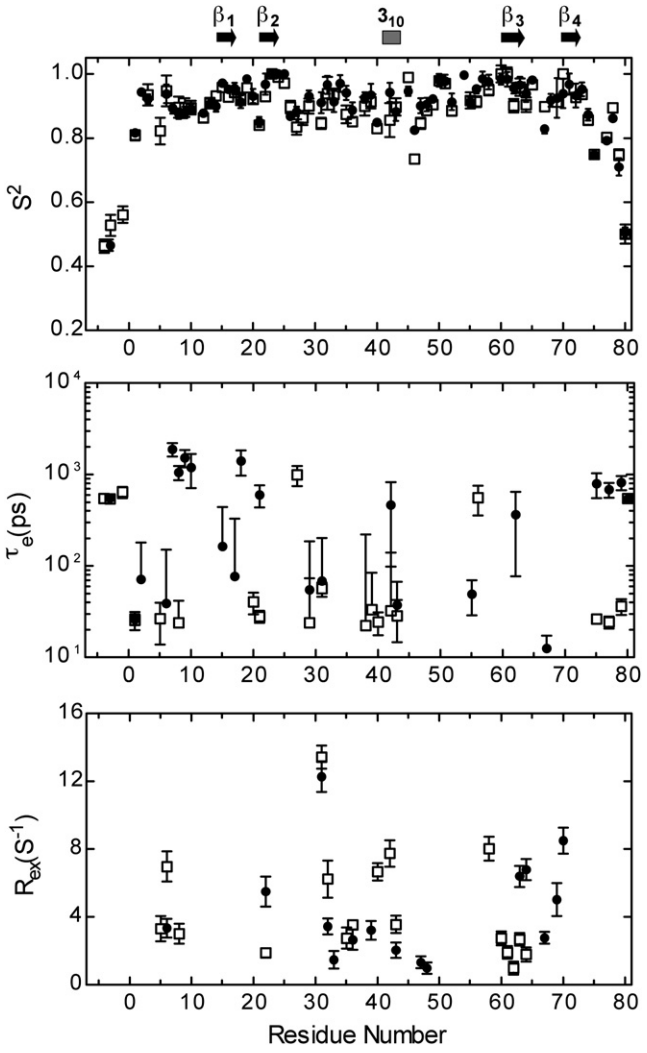

FIGURE 1 Residue-specific dynamics parameters calculated from the extended Lipari-Szabo model-free formalism for K2$_{Pg}$ in absence (*open squares*) and presence (*solid circles*) of VEK-30. Secondary structure elements are displayed above the top graph.

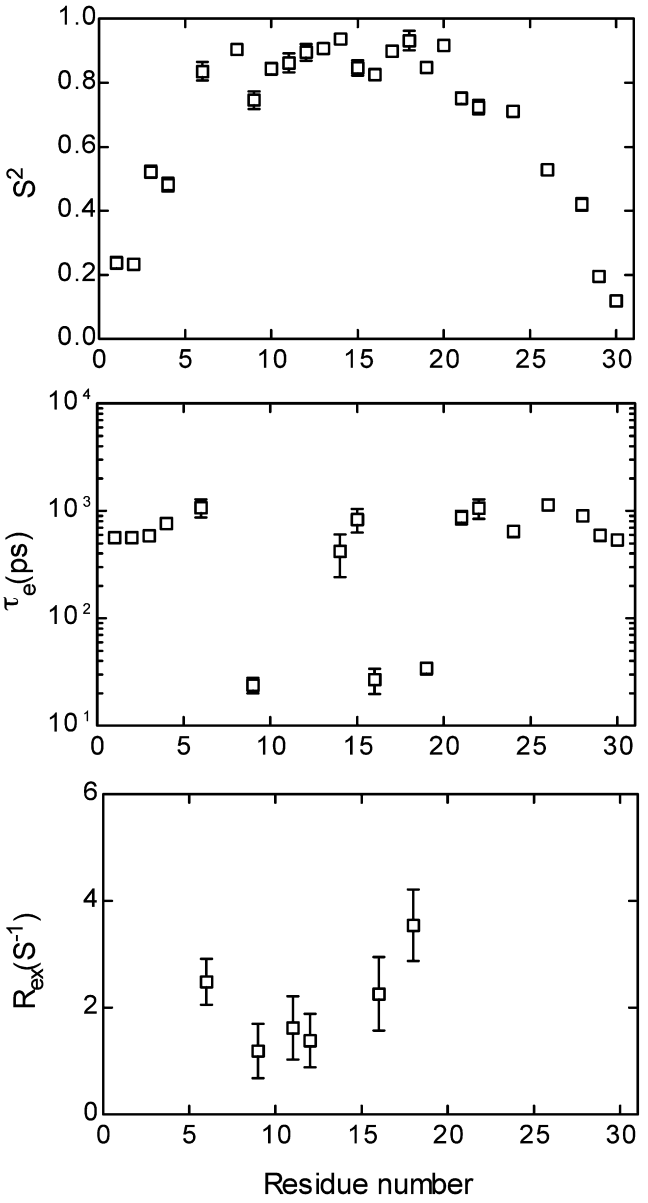

FIGURE 2 Residue-specific dynamics parameters calculated from the extended Lipari-Szabo Model-free formalism for VEK-30 binding to K2$_{Pg}$.

residues located within, or in close proximity to, the binding center of apo-K2$_{Pg}$, e.g., Cys^{50}, Arg^{51}, Arg^{58}, Trp^{60}, Cys^{61}, Thr^{63}, Asp^{65}, and Trp^{70}, exhibit relatively high order parameters, suggesting that low mobility in these positions likely plays a role in restricting the conformational changes required for complex formation.

A total of 21 and 23 residues of apo- and VEK-30 complexed K2$_{Pg}$, respectively, undergo fast internal motions on the ps-ns timescale, as shown by τ_e values in the range of 20–1000 ps (free) and 30–1900 ps (complexed). Most of these residues have surface-exposed side chains. For some residues outside this binding surface, the mobility of K2$_{Pg}$ on this timescale changes on binding to VEK-30. Notably, in the N-terminal electrostatic field region of Ser^{38}-Lys^{43}, more residues exhibit nonzero τ_e contributions for apo-K2$_{Pg}$ (five residues are accounted for with models 2 or 4 in apo-form whereas only two residues require τ_e contributions in bound form). This indicates that complexation of K2$_{Pg}$ with VEK-30 reduced those internal motions characterized by correlation times of 20–460 ps in this region. In addition, slow motions, as reflected by R_{ex} in the μs-ms timescale, are distributed throughout the backbone, especially around the binding sites of both forms (Fig. 3,*C* and *D*). In total, the R_{ex} parameter is required for 15 residues of bound K2$_{Pg}$, whereas 18 residues contain R_{ex} contributions in case of apo-K2$_{Pg}$. However, some differences were observed in several regions for conformational exchanges: 1), N-terminal residues Ser^5–Asn^8 showed conformational exchanges in apo-K2$_{Pg}$, whereas only Gly^6 exhibited conformational exchange in the bound form; 2), a number of conformational exchange contributions were observed in the N-termini of

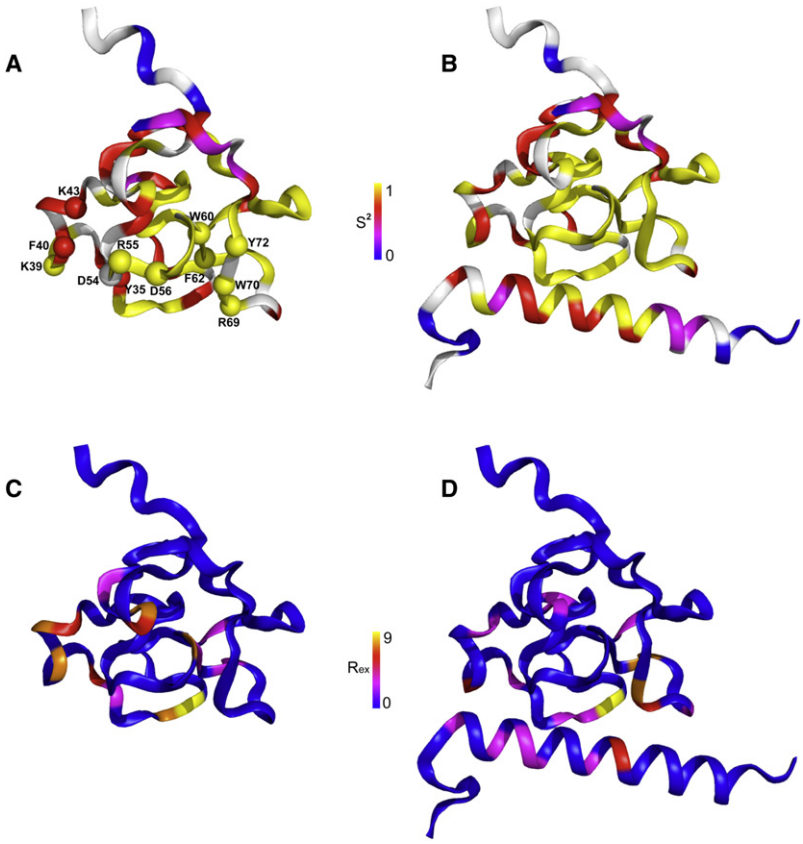

FIGURE 3 Mapping of the dynamics parameters on the protein structures both of free and bound forms with continuous-scale colors. (*A* and *B*). Ribbon diagrams of (*A*) apo-$K2_{Pg}$ and (*B*) VEK-30/$K2_{Pg}$ representing the generalized order parameter, S^2, with color coding as follows: blue, $0 < S^2 < 0.7$; magenta, $0.7 < S^2 < 0.8$; red $0.8 < S^2 < 0.9$; yellow, $0.9 < S^2 < 1$. Unanalyzed residues are white. (*C* and *D*) Ribbon diagrams of apo-$K2_{Pg}$ (*C*) and VEK-30/$K2_{Pg}$ (*D*) representing the conformational exchange dynamics on the μs-ms motional timescale, as indicated by R_{ex} (Hz). Color coding of R_{ex} is as follows: blue, R_{ex} ~0; magenta, $1 < R_{ex} < 3$; red, $3 < R_{ex} < 6$; orange, $6 < R_{ex} < 9$; yellow, $R_{ex} > 9$. Molecular models were drawn using the NMR average structure (PDB entry 2KJ4). The hydrophobic core, composed of Tyr^{35}, Phe^{40}, Trp^{60}, Phe^{62}, Trp^{67}, and Phe^{72}, and the anionic (Asp^{54} and Asp^{56}) and cationic (Lys^{39}, Lys^{43}, Arg^{55}, and Arg^{69}) centers are shown in spheres with labeled residues (the color coding of the spheres is the same as the dynamics parameters) in Fig. 3 *A*.

the interacting interface between $K2_{Pg}$ and VEK-30 (Ser^{34}–Lys^{43}) for both forms, but the free form showed a higher average value ($4.8 \pm 2.2\ s^{-1}$) than the bound form ($2.3 \pm 0.7\ s^{-1}$) in this region; 3), in the absence of VEK-30, Arg^{58}, a residue near the anionic center, exhibited significant conformational exchange. Further, the critical hydrophobic binding region Trp^{60}–Phe^{62}, also exhibited nonzero conformational exchange contributions. In contrast, these conformational exchanges substantially disappeared on binding to VEK-30, suggesting complexation reduces the low-frequency motions in the central binding region; and 4), VEK-30-bound $K2_{Pg}$ showed enhanced conformational exchange motions in the C-terminal binding region (Thr^{63}–Trp^{70}) compared to the free form. In particular, the binding sites at Arg^{69} and Trp^{70} had restricted internal motions in the free form, as reflected by the high S^2 value, whereas they displayed marked conformational exchange motions on binding to VEK-30, with R_{ex} of $5.0 \pm 0.9\ s^{-1}$ and $8.5 \pm 0.8\ s^{-1}$, respectively.

Model-free analysis of VEK-30 backbone motions in complex with $K2_{Pg}$

Relaxation data for the VEK-30/$K2_{Pg}$ complex was analyzed assuming that the overall rotational diffusion is isotropic. The dynamics model best describing the data for each residue in bound VEK-30 is shown in Fig. 2. The S^2 values for the N- and C-terminal residues are distinctly smaller than the S^2 values of other regions of the peptide. This indicates that both the N- and C-termini exhibit high mobility on the ps-ns timescale, which is consistent with relatively unstructured portions of the bound peptide. The average S^2 of the main binding region residues, 6–20, is 0.87 ± 0.05, indicating limited ps-ns timescale motion. In contrast, the average S^2 value for extended region of α-helix, segment 21–26, is 0.68 ± 0.10, which indicates that this region has increased mobility relative to the main binding region, perhaps due to the lack of contacts with $K2_{Pg}$. In addition to the two termini of the peptide, several residues, viz., Ala^6, Glu^9, Lys^{14}, Asn^{15}, Glu^{16}, Glu^{19}, Ala^{21}, Glu^{22}, Glu^{24}, and Leu^{26}, show fast and slow internal motions (τ_e) that occurred on a 20 ps to 1.2 ns timescale, which are characterized by the complex models 2, 4, and 5, respectively.

Chemical shift perturbation on complexation

We have measured 2D ^1H-^{15}N HSQC spectra of the peptide species involved in free and bound states (Fig. 4) to obtain direct insights into the effects of complex formation on protein structure due to the exquisite sensitivities of chemical shifts to the local environment. Fig. 5, *A* and *B*, shows the composite ^1H and ^{15}N chemical shift changes versus residue numbers, and the mapping of the chemical shift changes onto the structure of complex (Fig. 5 *C*). Relatively slight

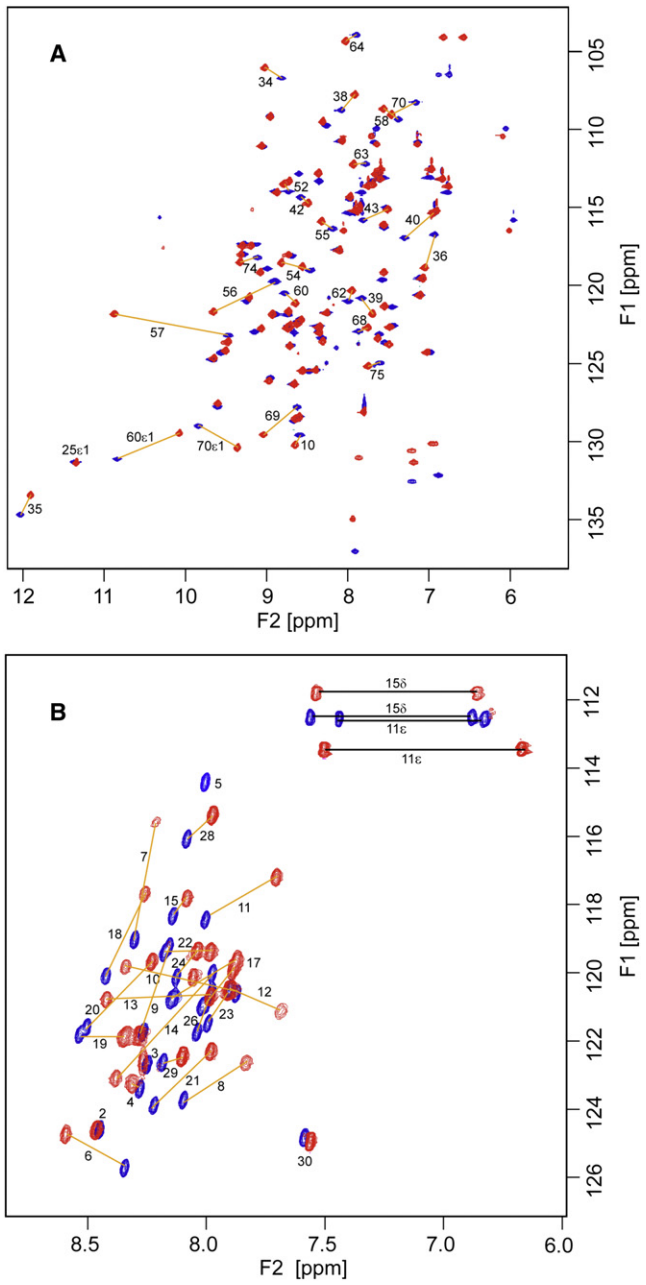

FIGURE 4 ^{1}[H]-^{15}N HSQC spectral analyses of (*A*) K2$_{Pg}$ and (*B*) VEK-30, respectively. Spectral shifts in the absence (*red*) and presence (*blue*) of VEK-30 (*A*) and in absence (*blue*) and presence (*red*) of K2$_{Pg}$ are superimposed. The residue numbers are labeled in the plots.

perturbations were observed for most residues of K2$_{Pg}$, which are spatially far from the ligand-binding sites. In contrast, pronounced perturbations occurred in the vicinity of several binding regions (Fig. 5 *C*). The K2$_{Pg}$ segments, Gly^{34}–Phe^{40}, Asp^{54}–Trp^{60}, and Arg^{69}–Trp^{70}, are the most sensitive to ligand binding, as revealed by the significantly perturbed chemical shifts (Fig. 5 *A*). They include residues located close to the hydrophobic (Gly^{34}, Tyr^{35}, Phe^{40}, Trp^{60}, Trp^{70}), cationic (Lys^{39}, Lys^{43}, Arg^{55}, R^{69}), and anionic (Asp^{54} and Asp^{56}) centers. Other residues exhibiting distinct binding-induced resonance shifts are Asp^{10}, Ser^{14}, Asp^{33}, Cys^{73}, and Ile^{75}, suggesting that residues far from the binding interface are affected by complexation. In addition, the side chain indole rings of Trp^{60} and Trp^{70} in the LBS also display chemical shift changes of aromatic NH$^{\varepsilon 1}$ resonances on binding VEK-30. Interestingly, a notable change was also observed for the side chain NH$^{\varepsilon}$ resonance of Arg^{69} (Fig. 4 *A*).

In case of VEK-30 binding to K2$_{Pg}$, almost all amide resonances of VEK-30 appeared in new positions in the HSQC spectra compared to uncomplexed VEK-30, except for the two termini (Val^{1}–Ser^{5} and Glu^{29}–Tyr^{30}) (Fig. 4 *B*). This shows that the majority of residues of VEK-30 display significant chemical-shift changes, demonstrating that their local environments were markedly affected on binding of K2$_{Pg}$ (Fig. 5 *C*). The residues of the helical region are divided into two groups. One group includes residues, which participate directly in binding, exhibit >0.2 ppm in its chemical perturbations. The most striking differences occurred in residues Asp^{7}, Glu^{9}, Leu^{10}, Leu^{13}, Lys^{14}, His^{18}, and Glu^{20}. Another group of residues exhibiting distinct differences in amide chemical shifts includes Ala^{8}, Gln^{11}, Arg^{12}, Asn^{15}, Glu^{16}, Glu^{19}, and the segment, Glu^{22}–Lys^{27}. The side chains of Gln^{11} and Asn^{15} also show significant differences in this regard (Fig. 4 *B*).

DISCUSSION

Whereas high-resolution structures of the complex of VEK-30/K2$_{Pg}$ have been determined, no detailed studies of the dynamics of this interaction have been carried out. This has now been accomplished in the current study.

The backbone relaxation data on K2$_{Pg}$, and the subsequent model-free analysis, show that most amino acid residues in both its apo and bound forms have relatively high order parameters despite a paucity of regular secondary structure in K2$_{Pg}$ (Figs. 1 and 3). This indicates that the backbone internal motions are highly restricted, and that K2$_{Pg}$ is a rigid molecule in both forms. This is consistent with reports for related kringle modules (20–22). The rigid structure and restricted dynamical properties seem to be a general feature of kringle modules and confirm other reports that concluded that the LBS was preformed in kringle domains.

Effect of VEK-30 binding on the K2$_{Pg}$

Our results show that the backbone dynamics of K2$_{Pg}$ are similar in the free and bound forms, but, nonetheless, interesting differences are present. We have analyzed these subtle differences in mobility based on known structural data, and conclude that by comparing the order parameters of free and bound K2$_{Pg}$, the binding of VEK-30 results in extensive increases and a lesser decreases in S^2, suggesting that binding of VEK-30 decreases the internal backbone motions

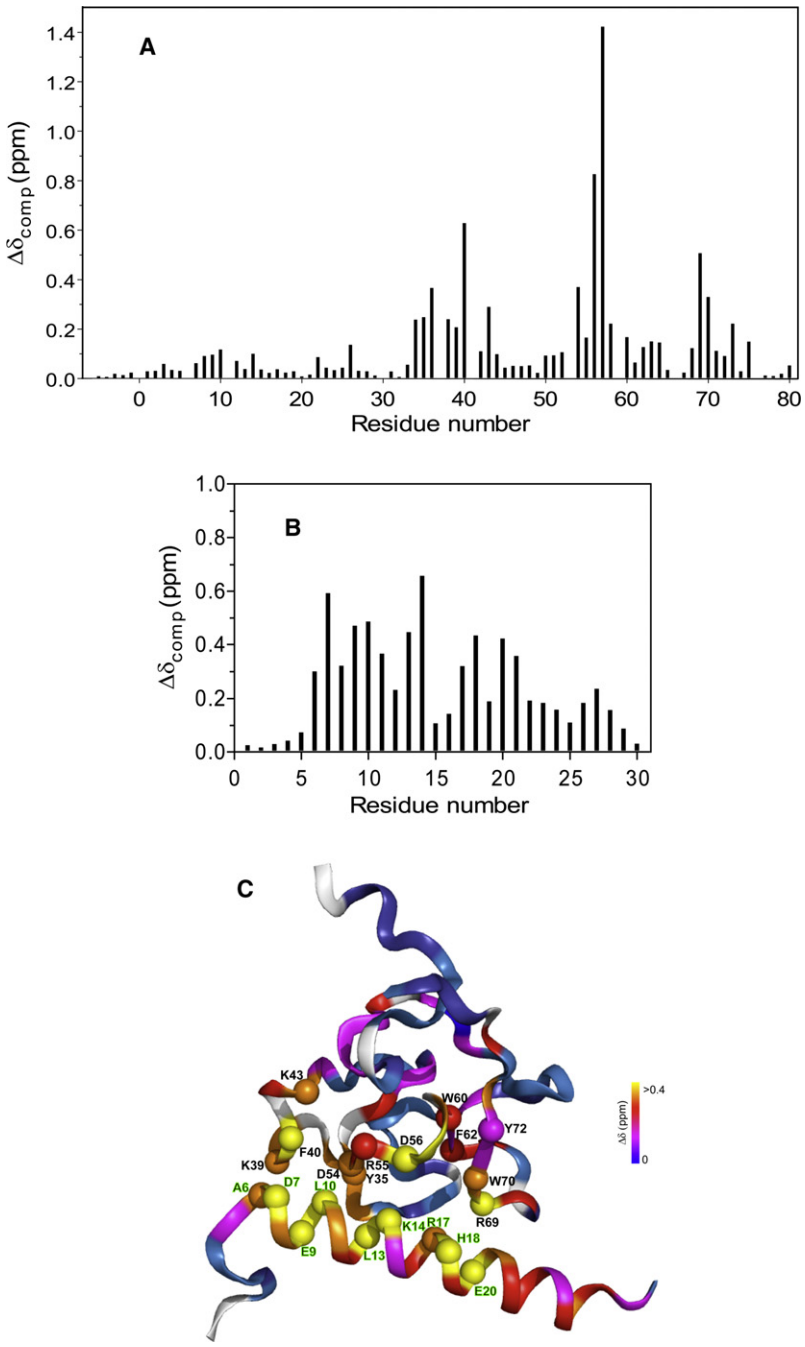

FIGURE 5 Chemical-shift differences between free and bound forms of $K2_{Pg}$ (*A*) and VEK-30 (*B*) as a function of the residue number. Chemical-shift changes were calculated by the equation, $\Delta\delta_{comp} = [(\Delta\delta_{HN})^2 + (\Delta\delta_N/6)^2]^{1/2}$, where $\Delta\delta_H$ and $\Delta\delta_N$ represent the chemical-shift changes of ^1H and ^{15}N atoms between free and bound forms, respectively. (*C*) Color mapping of the chemical shift differences on the NMR structure (PDB 2KJ4): dark blue, $\Delta\delta_{comp}$ ~0; light blue, $0.02 < \Delta\delta_{comp} < 0.06$; magenta, $0.06 < \Delta\delta_{comp} < 0.1$; red $0.1 < \Delta\delta_{comp} < 0.2$; orange, $0.2 < \Delta\delta_{comp} < 0.4$; yellow, $\Delta\delta_{comp} > 0.4$. Proline and unassigned residues are in white. The important binding sites in $K2_{Pg}$ are shown in spheres as in Fig. 3 *A*. The residues of VEK-30 directly involved in binding are also shown in spheres with corresponding color coding and labeled by green font.

of $K2_{Pg}$ (Fig. 6 and Fig. S4). A good example is noted in the region Tyr^{35}–Asn^{42}, which experiences relative higher amplitude motions on the ps-ns timescale in the apo-form (average $S^2 = 0.87$). Binding of VEK-30 causes a systematic increase in the S^2 of this region ($S^2 = 0.91$), suggesting that more restricted motions occur herein on VEK-30 binding. We also conclude that slow motions on the μs-ms scale are biologically important because they are close to the timescales of functional processes, such as docking and protein folding (23–25). The comparison of the dynamic behavior of free and bound $K2_{Pg}$ indicated that although high frequency internal motions were similarly observed in most residues of $K2_{Pg}$, conformational exchanges in μs-ms timescales observed at the binding face of free and VEK-30-bound $K2_{Pg}$, have some different distributions and/or distinct tendencies. Notably, Phe^{40}, Asn^{42}, Lys^{43}, Arg^{58}, and Trp^{60} have high R_{ex} values in apo-$K2_{Pg}$. However, on binding of VEK-30, these prominent conformational dynamics on the μs-ms timescale are attenuated, and even quenched, suggesting that the conformational flexibility at these sites likely contributes to the recognition of the ligand and is required for binding. In contrast, the VEK-30-bound $K2_{Pg}$

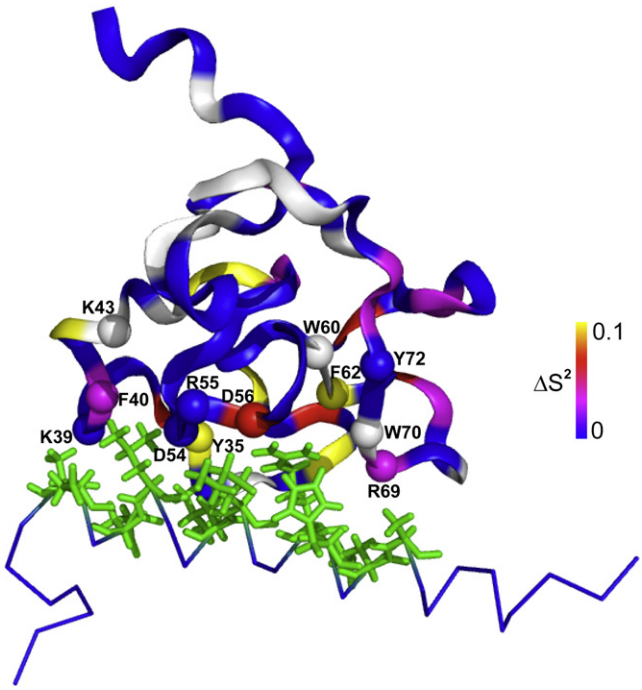

FIGURE 6 Effect of binding of VEK-30 on the generalized order parameter (S^2) of K2$_{Pg}$. $\Delta S^2 = S^2$ (after binding) $- S^2$ (before binding) and is mapped by continuous-scale color onto the structures. Positive ΔS^2 values denote enhanced rigidity of the protein backbone on binding. Residues with negative ΔS^2 values are white. The main chain of VEK-30 bound to K2$_{Pg}$ is shown as a green ribbon and the side chains of residues involved in interactions with K2$_{Pg}$ are represented as green sticks. Values of ΔS^2 are presented in Fig. S4. The important binding sites in K2$_{Pg}$ are shown in spheres, as in Fig. 3 *A*, and the color coding of spheres is the same as ΔS^2.

shows enhanced conformational exchange motions in the C-terminal binding region (Thr^{63}-Trp^{70}) compared to the free form. The increased mobility of residues on the μs-ms timescale, as a result of ligand binding, has been observed in other complex systems (26,27). For this system, both the crystal structure reported previously (5) and the NMR solution structure (6) of VEK-30 bound to K2$_{Pg}$ showed flexibility in the C-terminal binding region, especially two cationic resides, Lys^{68} and Arg^{69}, which manifest different orientations with their long side chains, resulting in different binding modes with the three anionic residues (Glu^{16}, Glu^{20}, and Glu^{24}) of VEK-30.

Comparison of the order parameters of free and bound K2$_{Pg}$ showed that, unexpectedly, not only residues in the binding region of K2$_{Pg}$, but also some residues located spatially far from the binding site were affected by complex formation (Fig. 6). However, besides these changes, some of the dynamical features of the free form are retained in the complex. Therefore, the structure of apo-K2$_{Pg}$ is comparatively rigid, but at the same time provides a relatively flexible interface for protein-ligand recognition. The flexibility at the binding interface is characteristic of the interaction surface of many proteins (28). The motions of residues in the vicinity of the binding interface are constricted in part by the binding of VEK-30, indicative of stabilization their internal motions.

Effect of K2$_{Pg}$ binding on dynamics properties of VEK-30

NMR spectral analysis showed that VEK-30 is unstructured and highly mobile in its apo form, whereas VEK-30 forms an extended regular α-helical structure when bound to K2$_{Pg}$. Here, we have shown that bound VEK-30 exhibits significantly different dynamical properties compared with free VEK-30. Interestingly, distinct backbone dynamical behavior is observed in different regions of the bound peptide, which correlate with specific interactions with K2$_{Pg}$. The residues at the two termini of VEK-30 have low S^2 values, whereas the majority of the helical residues in VEK-30 have relatively high order parameters. Mostly striking, the main binding region (residues 6–21) of VEK-30 displays the most restricted motion, reflected as the highest S^2 values. Analysis of the tertiary structure of VEK-30/K2$_{Pg}$ show many hydrophobic and electrostatic interactions in addition to the intermolecular hydrogen bonding, which may restrict the internal motions of this region. In contrast, the extended part of helix (residues 22–27) has relatively low order parameters and exhibits increased dynamics relative to the main binding portion of the helix (residues 6–21) of this peptide. This suggests that this region of the peptide experiences higher amplitude motions on a ps-ns timescale. This is consistent with the structure of the complex, which indicates little or no interactions of the C-terminal portion of VEK-30 with K2$_{Pg}$. Model-free analyses show that among the binding region residues (residues 6–21) of VEK-30, five residues are best fit by model 1, suggesting that this binding region exhibits a much simpler motion and is more immobilized on binding. At the same time, six nonzero R_{ex} and numerous τ_e contributions appeared, indicating that flexibility of the conformation of VEK-30 may be required for high-affinity and high-specificity of the binding. In summary, binding of VEK-30 to K2$_{Pg}$ results in widespread rigidification of the backbone in the extended helix (Ala^6–Lys^{27}) of VEK-30, despite the complex dynamics that exist in this region.

Comparison of the dynamics of other ligand/kringle interactions

The structures of kringle modules and their complexes with lysine analogs have been solved by both NMR and x-ray crystallographic methods (20,22,29–32). These structures reveal similar binding sites, involving hydrophobic and electrostatic interactions. Furthermore, dynamics studies show that they have similar patterns of internal motions on binding of lysine analogs (20,21,32). NMR spectra also indicated that almost no visible shifts are observed in kringle modules after binding of small lysine analogs, except for several

important binding sites (20,21). However, in contrast, our results show that more amide resonances of $K2_{Pg}$ in the HSQC spectrum appeared in new positions after binding to VEK-30. This indicates that $K2_{Pg}$ undergoes larger and more extensive perturbations when bound to VEK-30 compared to kringles bound to small lysine analogs, and likely involve exosite interactions distal from the LBS.

In addition to primary sequence alignments and structural comparisons, investigation of the dynamical behavior of different kringle domains, complexed with different ligands, contributes to explanations of the differences in binding affinities and binding specificities with these ligands, as well as the very tight and selective binding of VEK-30 to $K2_{Pg}$. Despite the similar dynamical patterns of kringles in some regions, $K2_{Pg}$ exhibited somewhat different dynamics at multiple timescales, which likely contribute to the differences in its binding specificity. Distinct from other kringle modules, which display nearly no change in the S^2 for apo- and lysine analog-bound states, the S^2 for $K2_{Pg}$ bound to VEK-30 is slightly increased compared with the apo-form, indicating that the binding of VEK-30 rigidifies $K2_{Pg}$ to some extent. Another major difference is seen for some residues near the binding site of kringle modules, especially at exosites of the LBS that were confirmed to be involved in interactions with VEK-30, and also contribute to the stability of the VEK-30/$K2_{Pg}$ according to our solution structural analysis and mutagenesis studies reported earlier (6). Backbone dynamics of apo-$K1_{Pg}$ reported previously did not show significant chemical exchanges at exosites of the LBS (21). However, our present results show that the exosite residues of LBS in $K2_{Pg}$, Tyr^{35}-Ile^{36}, Phe^{40}, Asn^{42}-Lys^{43}, Arg^{58}, and Cys^{61}–Thr^{64}, experience chemical exchanges with R_{ex} values of 1.0–8.0 s^{-1}. These differences with other kringle modules suggest that the newly identified exosites of $K2_{Pg}$ adopt more flexible conformations in the absence of ligand, thus allowing local structural rearrangements to accommodate the binding of larger- and longer-chain peptides, an important feature in explaining the high specificity of $K2_{Pg}$ binding to VEK-30.

We reported recently the solution structure of the VEK-30/$K2_{Pg}$ complex, and compared the structures of $K2_{Pg}$ bound to the small ligand, t-aminomethyl-cyclohexane-1-carboxylic acid (AMCHA) (6). The results showed that although the NMR structure of $K2_{Pg}$ in the VEK-30/$K2_{Pg}$ complex is similar to that of $K2_{Pg}$ bound to AMCHA, some subtle differences were observed in side chain geometries of several binding site residues. Most strikingly, two cationic residues, Lys^{39} and Lys^{43}, have distinctly different side chain orientations in the two complexes, and the topology of backbone in vicinity of Lys^{43} is distinctly different. Comparing the dynamics of the two ligand-bound systems, restricted motions on ps-ns timescales are fitted for residues Cys^{22}, His^{31}, His^{33}, Ile^{36}, Thr^{63}, Thr^{64}, and Trp^{70} of $K2_{Pg}$ with both ligands. However, consistent with their solution structures, the backbone dynamics also revealed some subtle differences. It is interesting to note that these residues have nonzero R_{ex} values in VEK-30/$K2_{Pg}$ (Lys^{39} and Lys^{43} show a value of 3.2 and 2.1 s^{-1}, respectively), but not in the AMCHA/$K2_{Pg}$ complex, indicating the VEK-30 bound $K2_{Pg}$ displays more complex motions in these regions. In addition, comparisons of ligand-bound $K2_{Pg}$ structures show that the aromatic ring of Phe^{40} in VEK-30/$K2_{Pg}$ is a somewhat closer to the ligand center, such that it makes hydrophobic contacts with the methyl groups of Leu^{10} and Leu^{13} of VEK-30. By investigating the dynamical behavior of Phe^{40} in two complexed states, it is seen that this residue experiences flexible motions at the ps timescale, characterized by a relatively low order parameter (S^2 of Phe^{40} is 0.77, whereas the overall generalized S^2 of $K2_{Pg}$ is 0.85), when complexed to AMCHA. In contrast, this residue becomes considerably more rigid on binding of VEK-30, displaying a higher S^2 value of 0.85. This is consistent with the fact Phe^{40} directly participates in this binding event in the complex of VEK-30/$K2_{Pg}$, but not in the complex of AMCHA/$K2_{Pg}$ (6).

An additional significant difference is observed in the C-terminal binding region of $K2_{Pg}$. In the AMCHA/$K2_{Pg}$ complex, only Trp^{70} exhibits conformational exchange on μs-ms timescale, whereas three residues, specifically, Asn^{67}, Arg^{69}, and Trp^{70}, have significant conformational exchange rates when bound to VEK-30. There are some structural differences in the orientations of side chains of binding site residues, Ly^{s68} and Arg^{69}, due to the different interactions involved. This impacts the mobility of binding sites and vicinal residues. These differences are also reflected in HSQC spectra of $K2_{Pg}$ by comparison of chemical shift perturbations derived from binding of different ligands. Because the $K2_{Pg}$ used in these two complexes has a single site mutation at position 72 (Tyr^{72} and Leu^{72} are present in VEK-30/$K2_{Pg}$ and AMCHA/$K2_{Pg}$, respectively), the above differences in the region of Asn^{67}–Trp^{70} could be due to the effects of this mutation. In this regard, the EACA/$K1_{Pg}$, AMCHA/$K1_{Pg}$, and EACA/KIV_8 complexes were investigated regarding relaxation data in this region, which have the same residue, Tyr^{72}, and are bound to the same or similar lysine analogs (21,22,32). However, the residues in this region did not exhibit chemical exchanges of high magnitude for any of these kringle/ligand systems. Therefore, the possible influence of the Leu^{72}Tyr mutation is excluded in the VEK-30/$K2_{Pg}$ complex and these substantial differences of backbone dynamics in this region are likely attributable to the different docking modes between lysine analogs and VEK-30.

The dynamical behavior of each component of the VEK-30 and $K2_{Pg}$ in their apo- and bound forms, and the dynamical comparisons with different kringle-ligand systems, together with our previous structural and mutagenesis studies, enable us to further probe the correlation between the dynamics and binding of VEK-30 bound to $K2_{Pg}$. As shown in Fig. 5 *C*, the major binding interactions in

VEK-30/$K2_{Pg}$ occur between each face of VEK-30 and $K2_{Pg}$. First, an exposed hydrophobic groove, consisting of Tyr^{35}, Phe^{40}, Trp^{60}, Tyr^{62}, Trp^{70}, and Tyr^{72}, extends throughout the binding interface, and correspondingly, several hydrophobic side chains of VEK-30, Ala^{6}, Leu^{10}, Leu^{13}, Arg^{17}, and Ala^{21}, are buried within this groove, resulting in a broad hydrophobic interface between $K2_{Pg}$ and VEK-30. Additionally, residues Asp^{54} and Asp^{56} of $K2_{Pg}$ form an anionic locus interacting with Lys^{14}, Arg^{17}, and His^{18} of VEK-30. Also, Arg^{69} of $K2_{Pg}$ acts as a C-terminal cationic locus interacting with Glu^{16} and Glu^{20} of VEK-30. The above extensive hydrophobic and ionic interactions were verified to be important to stabilization of the complex through site-specific mutagenesis studies (5), thus providing the molecular basis of the high affinity. These dynamical analyses show that, for $K2_{Pg}$, most of these binding sites and their vicinal residues undergo comparatively restricted motions in the ps-ns timescale in both apo- and its VEK-30 bound form. This indicates that the broad hydrophobic groove and the central and C-terminal electrostatic fields are both preformed and sufficiently rigid, to allow the $K2_{Pg}$ binding site to accommodate the VEK-30 peptide. Interestingly, some residues near Arg^{69} exhibit significant chemical exchange processes on binding of VEK-30, thus providing possibilities to interact with the carboxyl moiety of Glu residues of VEK-30 through local conformational adjustments in this region. Additionally, in the N-terminus of the interface, the exosites of the LBS, Lys^{39}, Lys^{43}, and Arg^{55} of $K2_{Pg}$, engage the N-terminus of VEK-30 by electrostatic and hydrogen bond interactions with negatively charged residues, Asp^{7} and Glu^{9}, of VEK-30, forming a sandwich electrostatic field. Our previous site-specific mutagenesis studies confirmed that this electrostatic field plays an additional important role in the binding of VEK-30 to $K2_{Pg}$ (6). However, these dynamical studies show that the N-terminal cationic locus and its vicinal residues in apo-$K2_{Pg}$ experience relative flexible internal motions on the ps-ns timescale and even higher amplitude chemical exchange processes on the μs-ms timescale, and these motions are stabilized after VEK-30 docks to $K2_{Pg}$. That this phenomena did not occur in a related region of other kringle modules, suggests that these dynamical processes in the N-terminal interface play a role in the specific recognition of VEK-30 by $K2_{Pg}$.

In summary, whereas $K2_{Pg}$ is relatively rigid with a preformed LBS, this allows only a basal level of binding to small molecules. A larger ligand, e.g., VEK-30, is a highly mobile and unstructured peptide in the absence of $K2_{Pg}$, suggesting that the binding of VEK-30 to $K2_{Pg}$ results in a decreased entropy for both the VEK-30 and $K2_{Pg}$. Although it would be energetically unfavorable, presumably the flexibility in the unbound form allows the protein to maximize the binding enthalpy at the extended interface, overcoming the unfavorable entropic contribution. The flexibility of the peptide ligand and some of the exosite residues of $K2_{Pg}$ allow for additional binding energy as compared to small molecule ligands, thus explaining on a dynamic level the tight and specific binding of VEK-30 to human $K2_{Pg}$.

SUPPORTING MATERIAL

Four figures are available at http://www.biophysj.org/biophysj/supplemental/S0006-3495(10)00484-4.

This work was supported by the National Institutes of Health (HL013423).

REFERENCES

1. Berge, A., and U. Sjöbring. 1993. PAM, a novel plasminogen-binding protein from *Streptococcus pyogenes*. *J. Biol. Chem.* 268:25417–25424.
2. Sun, H., U. Ringdahl, …, D. Ginsburg. 2004. Plasminogen is a critical host pathogenicity factor for group A streptococcal infection. *Science.* 305:1283–1286.
3. Wistedt, A. C., H. Kotarsky, …, U. Sjöbring. 1998. Kringle 2 mediates high affinity binding of plasminogen to an internal sequence in streptococcal surface protein PAM. *J. Biol. Chem.* 273:24420–24424.
4. Wistedt, A. C., U. Ringdahl, …, U. Sjøbring. 1995. Identification of a plasminogen-binding motif in PAM, a bacterial surface protein. *Mol. Microbiol.* 18:569–578.
5. Rios-Steiner, J. L., M. Schenone, …, F. J. Castellino. 2001. Structure and binding determinants of the recombinant kringle-2 domain of human plasminogen to an internal peptide from a group A Streptococcal surface protein. *J. Mol. Biol.* 308:705–719.
6. Wang, M., J. Zajicek, …, F. J. Castellino. 2010. Solution structure of the complex of VEK-30 and plasminogen kringle 2. *J. Struct. Biol.* 169:349–359.
7. Clackson, T., and J. A. Wells. 1995. A hot spot of binding energy in a hormone-receptor interface. *Science.* 267:383–386.
8. Kay, L. E., D. R. Muhandiram, …, J. D. Forman-Kay. 1998. Correlation between binding and dynamics at SH2 domain interfaces. *Nat. Struct. Biol.* 5:156–163.
9. Wang, C., N. H. Pawley, and L. K. Nicholson. 2001. The role of backbone motions in ligand binding to the c-Src SH3 domain. *J. Mol. Biol.* 313:873–887.
10. Farrow, N. A., R. Muhandiram, …, L. E. Kay. 1994. Backbone dynamics of a free and phosphopeptide-complexed Src homology 2 domain studied by ^{15}N NMR relaxation. *Biochemistry.* 33:5984–6003.
11. Gagné, S. M., S. Tsuda, …, B. D. Sykes. 1998. Backbone and methyl dynamics of the regulatory domain of troponin C: anisotropic rotational diffusion and contribution of conformational entropy to calcium affinity. *J. Mol. Biol.* 278:667–686.
12. Spyracopoulos, L., S. M. Gagné, …, B. D. Sykes. 1998. Dynamics and thermodynamics of the regulatory domain of human cardiac troponin C in the apo- and calcium-saturated states. *Biochemistry.* 37: 18032–18044.
13. Mittermaier, A., and L. E. Kay. 2006. New tools provide new insights in NMR studies of protein dynamics. *Science.* 312:224–228.
14. Lipari, G., and A. Szabo. 1981. Nuclear magnetic resonance relaxation in nucleic acid fragments: models for internal motion. *Biochemistry.* 20:6250–6256.
15. Lipari, G., and A. Szabo. 1982. Model-free approach to the interpretation of nuclear magnetic-resonance relaxation in macromolecules.1. Theory and range of validity. *J. Am. Chem. Soc.* 104:4546–4559.
16. Lipari, G., and A. Szabo. 1982. Model-free approach to the interpretation of nuclear magnetic-resonance relaxation in macromolecules.2. Analysis of experimental results. *J. Am. Chem. Soc.* 104:4559–4570.
17. Markley, J. L., A. Bax, …, K. Wüthrich, IUPAC-IUBMB-IUPAB Inter-Union Task Group on the Standardization of Data Bases of Protein and Nucleic Acid Structures Determined by NMR Spectroscopy. 1998.

Recommendations for the presentation of NMR structures of proteins and nucleic acids. *J. Biomol. NMR.* 12:1–23.

18. Dosset, P., J. C. Hus, …, D. Marion. 2000. Efficient analysis of macromolecular rotational diffusion from heteronuclear relaxation data. *J. Biomol. NMR.* 16:23–28.
19. Mandel, A. M., M. Akke, and A. G. Palmer, 3rd. 1995. Backbone dynamics of *Escherichia coli* ribonuclease HI: correlations with structure and function in an active enzyme. *J. Mol. Biol.* 246:144–163.
20. Marti, D. N., J. Schaller, and M. Llinás. 1999. Solution structure and dynamics of the plasminogen kringle 2-AMCHA complex: 3(1)-helix in homologous domains. *Biochemistry.* 38:15741–15755.
21. Zajicek, J., Y. Chang, and F. J. Castellino. 2000. The effects of ligand binding on the backbone dynamics of the kringle 1 domain of human plasminogen. *J. Mol. Biol.* 301:333–347.
22. Chitayat, S., V. Kanelis, …, S. P. Smith. 2007. The plasma lipoprotein lipoprotein(a) [Lp(a)] comprises a low-density lipoprotein (LDL)-like particle covalently attached to the glycoprotein apolipoprotein(a). *Biochemistry.* 46:1732–1742, [apo(a)].
23. Akke, M., R. Bruschweiler, and A. G. Palmer. 1993. NMR order parameters and free energy: an analytical approach and its application to cooperative Ca^{2+} binding by calbindin D9K. *J. Am. Chem. Soc.* 115:9832–9833.
24. Kalodimos, C. G., N. Biris, …, R. Kaptein. 2004. Structure and flexibility adaptation in nonspecific and specific protein-DNA complexes. *Science.* 305:386–389.
25. Keramisanou, D., N. Biris, …, C. G. Kalodimos. 2006. Disorder-order folding transitions underlie catalysis in the helicase motor of SecA. *Nat. Struct. Mol. Biol.* 13:594–602.
26. Kay, L. E., D. R. Muhandiram, …, J. D. Forman-Kay. 1996. Correlation between dynamics and high affinity binding in an SH2 domain interaction. *Biochemistry.* 35:361–368.
27. Stivers, J. T., C. Abeygunawardana, and A. S. Mildvan. 1996. ^{15}N NMR relaxation studies of free and inhibitor-bound 4-oxalocrotonate tautomerase: backbone dynamics and entropy changes of an enzyme upon inhibitor binding. *Biochemistry.* 35:16036–16047.
28. Luque, I., and E. Freire. 2000. Structural stability of binding sites: consequences for binding affinity and allosteric effects. *Proteins-Structure Function and Genetics.* (Suppl. 4):63–71.
29. Rejante, M. R., and M. Llinás. 1994. Solution structure of the epsilon-aminohexanoic acid complex of human plasminogen kringle 1. *Eur. J. Biochem.* 221:939–949.
30. Mathews, I. I., P. Vanderhoff-Hanaver, …, A. Tulinsky. 1996. Crystal structures of the recombinant kringle 1 domain of human plasminogen in complexes with the ligands ε-aminocaproic acid and *trans*-4-(aminomethyl)cyclohexane-1-carboxylic acid. *Biochemistry.* 35:2567–2576.
31. Chang, Y., I. Mochalkin, …, F. J. Castellino. 1998. Structure and ligand binding determinants of the recombinant kringle 5 domain of human plasminogen. *Biochemistry.* 37:3258–3271.
32. Battistel, M. D., A. Grishaev, …, M. Llinás. 2009. Solution structure and functional characterization of human plasminogen kringle 5. *Biochemistry.* 48:10208–10219.